Results in Engineering 30 (2026) 110094

Contents lists available at ScienceDirect

Results in Engineering

journal homepage: www.sciencedirect.com/journal/results-in-engineering

Significance of Cattaneo-Christov heat flux and bioconvection in magnetized Jeffrey nanofluid inside an extendable cylinder: Advanced in cooling system

Muhammad Jawad [a,*], Ali B.M. Ali [b], Aaqib Majeed [a], Narinderjit Singh Sawaran Singh [c], Abdul Kareem Abdul Jawwad [d], Hakim AL Garalleh [e], Ibrahim Mahariq [f,g,h,i,*]

[a] Department of Mathematics, Physics & Statistics, The University of Faisalabad, Faisalabad 38000, Pakistan
[b] Advanced Technical College, University of Warith Al-Anbiyaa, Karbala, Iraq
[c] Faculty of Data Science and Information Technology, INTI International University, Persiaran Perdana BBN, Putra Nilai, Nilai 71800, Malaysia
[d] Industrial Engineering Department, University of Jordan, Amman 11942, Jordan
[e] Department of Mathematical Science, College of Engineering, University of Business and Technology, Jeddah 21361, Saudi Arabia
[f] College of Engineering and Architecture, Gulf University for Science and Technology, Mishref, Kuwait
[g] Najjad Zeenni Faculty of Engineering, Al-Quds University, Jerusalem, Palestine
[h] Department of Electrical and Electronic Engineering, Faculty of Engineering and Architecture, Istanbul Gelisim University, Avcılar- Istanbul, 34310, Istanbul, Türkiye
[i] University College, Korea University, Seoul 02481, South Korea

ARTICLE INFO

Keywords:
Nanofluid
Non-Newtonian
Cylindrical surface
Bioconvection
Cattaneo-Christov heat

ABSTRACT

Owing to the exceptional thermal properties of non-Newtonian nanofluids, nanomaterials have reported widespread use in numerous fields such as mechanical engineering, cooling technologies, solar energy systems and industrial processes. This work aims to scrutinize the thermal behavior of Jeffrey nanofluids under the impact of bioconvection caused by gyrotactic microorganisms, with specific attention on the flow over an elongating cylinder. The inclusive innovation of this study lies in the incorporation of non-Fourier heat conduction modeled using the Cattaneo–Christov heat formulation instead of Fourier's law. Appropriate similarity functions are applied to renovate the governing equations into transformed ordinary differential equations. Numerical simulations are carried out using bvp4c solver via MATLAB, and the outcomes are compared with published studies to authenticate accuracy. Graphical illustrations are used to estimate the inspiration of key fluid parameters such as magnetic parameter $0.2 \leq M \leq 2.2$, curvature parameter $0 \leq \gamma \leq 0.8$, Jeffrey fluid $0.5 \leq \beta \leq 2.5$, Lewis number $1.2 \leq Le \leq 2.0$, buoyancy ratio parameter $0.5 \leq Nr \leq 2.5$, thermophoresis $0.1 \leq Nt \leq 1.0$ and bioconvective Lewis number $0.2 \leq Lb \leq 1.0$. It is witnessed that the velocity distribution rises with the curvature parameter and decreases with the Jeffrey, buoyancy ratio parameter and magnetic parameters. The thermal profile drops with growing thermal relaxation parameters, while it rises with both the magnetic parameter M and thermophoresis parameter Nt. The concentration and density profiles reduce with improving values of the Lewis number Le and bioconvective Lewis number Lb, respectively.

1. Introduction

Due to the widespread thermal applications of nanoparticles, investigators have studied their use in numerous industrial processes, engineering systems and useful real-world challenges. Modern developments in nanotechnology have initiated nanoparticles with enriched thermal properties, presenting efficient solutions to numerous problems related to low-cost energy alternatives. Likewise, metallic nanoparticles hold important promise in the medical field, containing applications such as brain tumor therapy, heart disease treatment, artificial lung development, disease diagnosis and cancer tissue destruction. The incorporation of nanomaterials with base liquids has also led to solar energy systems, thermal engineering processes and enhancements in cooling technologies. Nanoparticles classically have diameters smaller than 100 nm (Fig. 1a).

An innovative study on nanofluids was accomplished by Choi [1],

* Corresponding authors.
E-mail addresses: muhammadjawad.math@tuf.edu.pk (M. Jawad), maharik.i@gust.edu.kw (I. Mahariq).

https://doi.org/10.1016/j.rineng.2026.110094
Received 9 September 2025; Received in revised form 24 February 2026; Accepted 13 March 2026
Available online 15 March 2026

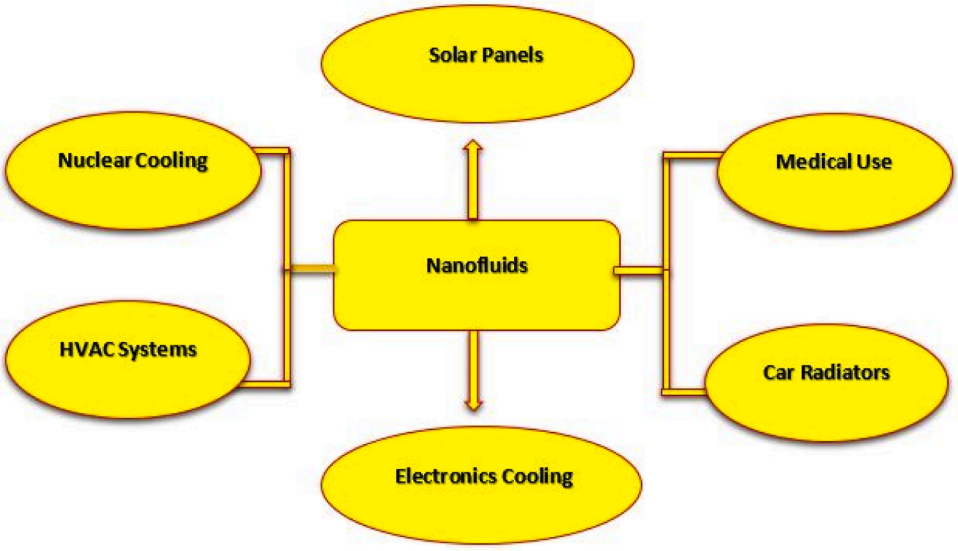

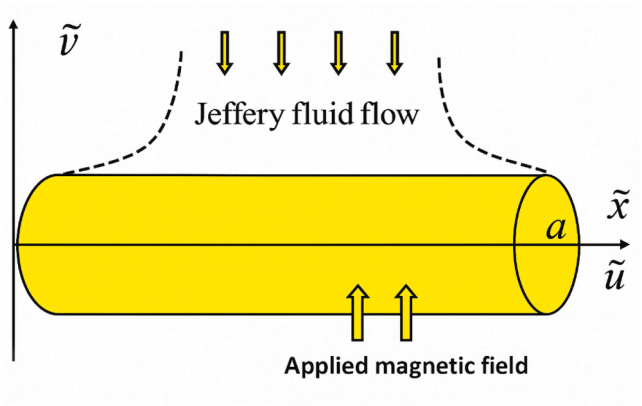

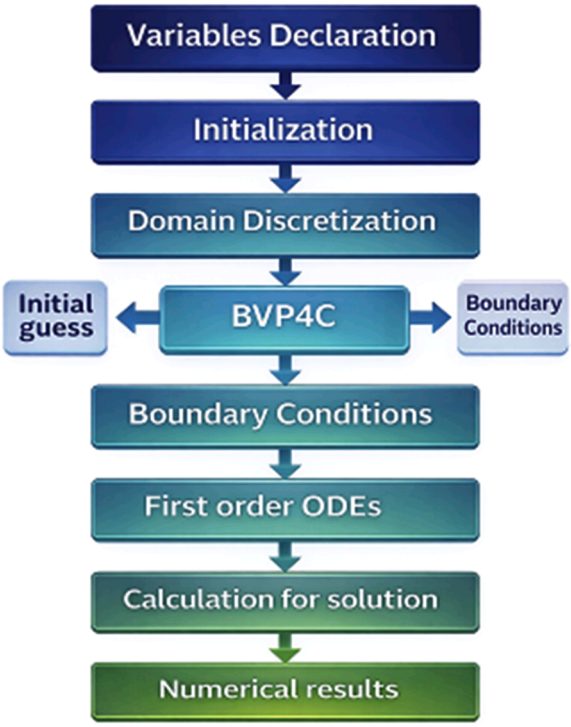

Fig. 1. a: Applications of nanofluid. b: Problem Geometry. c: bvp4c flow chart.

emphasizing the potential of these small materials. Vahidhosseini et al [2] presented the magnetic effects for nanofluid. Upreti et al [3] discussed the Cattaneo–Christov heat and magnetic effects for electromagnetics nanofluid due to shrinking/stretching surface. Sahamifar et al [4] perceived the nanofluid objects for thermal conductivity via interferometric method. Akbar et al [5] deliberated the thermal properties of radiative nanofluid with porous media and viscous dissipation. They found that growing the permeability parameter leads to a significance decline in system entropy. Non-Newtonian nanofluids are fluids that combine non-Newtonian base fluids with floating nanoparticles to enrich thermal and rheological characteristics. These fluids are used in advanced heat transmission, drug delivery unit, biomedical, polymer processing, food industry and industrial applications. Ketchup, toothpaste, yogurt, honey, cosmetic creams, paint, mayonnaise, shampoo, slime, molasses, blood, glue and whipped cream are some examples of non-Newtonian [6,7]. In recent years, scientists have developed nanofluid studies to non-Newtonian fluids owing to their noticeable rheological behavior and significance in industrial and engineering processes. To accurately attain the performance of such fluids, various non-Newtonian models have been occupied in nanofluid studies. These include Jeffrey nanofluids, Casson nanofluids, Carreau nanofluids and Bingham plastic nanofluids. These models allow investigators to superior understand and enhance the heat and mass transmission properties of nanofluids in engineering, technology and biological systems [8–10]. Chemically reactive Williamson fluid with viscous dissipation effects induced by curved surface was explored by Bahman et al

[11]. Thermal advancement in cross by using chemical reaction effect was premeditated by Salahuddin et al [12]. With the use of Cattaneo–-Christov heat, Algehyne et al. [13] presented a thermal development in Maxwell nanofluids. Among these, Jeffrey nanofluid models has increased interest for their capability to capture the elastic and viscous behavior of real fluids, making them appropriate for medical, manufacturing and polymer-based heat transfer applications [14,15]. Geometric configurations such as cylindrical surfaces are of specific importance due to their consequence in real-world systems like nuclear fuel rods, wires, pipes, reactors, heat exchangers, inkjet printing heads, rotating drums, cooling channels in turbines, oil and gas pipelines, geothermal boreholes, filtration units, cable insulation systems, industrial rollers, biomedical catheters and cylindrical electronic components. The analysis of nanofluid flow over or around cylindrical bodies deals vital insights for enriching heat dissipation in such systems [16,17]. Puneeth et al [18] travelled the significance of Thompson slip for nanofluid flow over cylinder. Sreenivasa et al [19] researched the heat transfer phenomena due to stretched cylinder in ferromagnetic nanofluid. Munir and Turabi [20] highlighted the thermal performance in hybrid nanofluid with inclined magnetic field bounded by cold cylinder. Zhao et al [21] demonstrated the mechanisms of improves thermal conductivity in electromagnetics nanofluid flowing due to spinning cylinder. Mebarek-Oudina et al [22] considered the internal heat generation and absorption effects in Burgers' fluid subjected to elongating cylinder. Junaid et al [23] conferred the thermal behavior of Jeffrey nanofluid with entropy generation induced by extending cylinder. Further, the relevance of cylindrical surface in engineering and thermal systems were studied by [24,25]. In addition to nanoparticles, the existence of motile microorganisms has become a considerable focus in bioconvective nanofluid enquiries. These micro germs, capable of spinning upward due to gravitational and viscous torques, improve the stability and mixing of colloidal systems. Their inclusion into nanofluid systems is especially vital in relevance such as biosensor technologies, microfluidic devices, biomedical diagnostics, wastewater treatment and biofuel production, where biological activity relates with heat and mass transfer mechanisms [26]. Ali et al [27] inspected analysis of heat transfer due to gyrotactic microorganisms suspended in powell-eyring nanofluid. Sarfraz et al [28] accompanied a stability analysis to check the role of gyrotactic microbes suspended in Jeffrey fluid flow due to biaxially elongating surface. Hussain et al. [29] considered the significance of bio-convection of motile micro germs merged in non-Newtonian nanofluid through horizontal plate. Bilal et al [30] travelled the impact of viscous dissipation and motile micro germs in electromagnetics Carreau fluid inside elongating cylinder. Sun et al [31] surveyed the role of bioconvection in electromagnetics flow of nanofluid prompted by permeable sheet. Khan et al [32] studied the heat transfer examination in radiative Eyring Powell fluid with temporal stability analysis. Hussain et al [33] explored the motile micro germs and wall temperature in fluid flow over absorbent plate with activation energy for engineering applications. Baithalu et al [34] reconnoitered the sway of entropy in hybrid nanofluid induced by heated surface. Loganathan et al [35] deliberated the impression of Riga surface and entropy generation on Maxwell nanofluid with importance of bioconvection. Reddy et al [36] travelled the sway of suction/injection and Cattaneo–Christov heat in electromagnetic nanofluid with entropy generation. Reddy et al [37] intended the applications of heat transmission using magnetic field in magnetized nanfluid due to square cavity.

The available literature review shows that bioconvective flow of non-Newtonian nanofluid due to an extendable sheet has been extensively discussed in the presence of various thermal effects. However, relatively limited attention has been given to the bio-convective flow of Jeffrey nanofluids containing swimming micro-germs and convective boundaries over an extendable cylinder. Therefore, the goal of this analysis is to examine the effects of a magnetic field and Cattaneo-Christov heat flux in Jeffrey nanofluid flow due to an extendable cylinder. The impact of buoyancy ratio, thermophoresis, bioconvection Rayleigh number, and Brownian motion are also considered. The freshness of this study lies in incorporating the combined influence of magnetic and Cattaneo-Christov heat flux effects in a Jeffrey nanofluid with buoyancy forces, which has not been comprehensively addressed before. The limitations of the present model are discussed to provide a foundation for future investigations involving more complex geometries and boundary conditions. These contributions place the current work in the context of the wider body of nanofluid research that builds up upon the classic research done by Choi [1] to non-Newtonian bioconvective systems controlled by an electromagnetic field and non-Fourier heat transfer. Direct usages of the results may be found in the high-tech cooling systems, biomedical apparatus, and environmental engineering systems.

2. Problem statement

The bioconvection flow of Jeffrey nanofluid subjected to stretchable cylinder with radius a is examined. The magnitude of motile microorganisms with buoyancy forces are deliberated in this work. The further flow assumption are outlined as (see Fig. 1b):

- The fluid is incompressible and axisymmetric, with constant density and no variation in the angular path around the cylinder.
- The flow is steady and laminar, meaning it is smooth, time-dependent, and free of turbulence.
- Heat transfer follows the Cattaneo–Christov model, a non-Fourier approach that accounts for thermal relaxation effects.
- The fluid is a Jeffrey-type, electrically conducting fluid exposed to a magnetic field, incorporating magnetohydrodynamic (MHD) interactions.
- The presence of motile microorganisms is included, influencing both thermal conductivity and mass transfer, relevant in bioconvective transport.
- Accomplishes of buoyancy forces, Brownian motion, and thermophoresis are considered to capture the influence of temperature and concentration gradients on nanoparticle dynamics.

The rheological equations of proposed non-Newtonian fluid are designed as follow:

$$\tau = -P\mathbf{I} + \mathbf{S}, \tag{1}$$

$$\mathbf{S} = \left(\frac{\mu}{1+\lambda_1}\right)\left[\mathbf{A}_1 + \lambda_2 \frac{D\mathbf{A}_1}{Dt}\right], \tag{2}$$

$$\left(\mathbf{A}_1 = \nabla\mathbf{V} + (\nabla\mathbf{V})^T\right), \tag{3}$$

The governing equations are designated as [38–43]:
Equation of Continuity

$$\frac{\partial(ru)}{\partial x} + \frac{\partial(rv)}{\partial r} = 0, \tag{4}$$

Equation of momentum

$$u\frac{\partial u}{\partial x}+v\frac{\partial u}{\partial r}=\frac{\mu}{\rho(1+\lambda_1)}\left[\frac{\partial^2 u}{\partial r^2}+\frac{1}{r}\frac{\partial u}{\partial r}+\lambda_2\left(v\frac{\partial^3 u}{\partial r^3}+\frac{\partial u}{\partial r}\frac{\partial^2 u}{\partial x\partial r}+u\frac{\partial^3 u}{\partial x\partial r^2}+\frac{u}{r}\frac{\partial^2 u}{\partial x\partial r}+\frac{v}{r}\frac{\partial^2 u}{\partial r^2}+\frac{\partial v}{\partial r}\frac{\partial^2 u}{\partial r^2}\right)\right]$$
$$-\frac{\sigma B_0^2}{\rho}u+\frac{1}{\rho_f}\begin{bmatrix}(1-C_\infty)\,g\;\;(T-T_\infty)\beta\rho_f-\\(\rho_p-\rho_f)g(C-C_\infty)\\-\gamma(N-N_\infty)\;(\rho_m-\rho_r)\end{bmatrix}, \tag{5}$$

Equation of Temperature

$$u\frac{\partial T}{\partial x}+v\frac{\partial T}{\partial r}+\lambda_E\left[u^2\frac{\partial^2 T}{\partial x^2}+v^2\frac{\partial^2 T}{\partial r^2}+2uv\frac{\partial^2 T}{\partial x\partial r}+u\frac{\partial v}{\partial x}\frac{\partial T}{\partial r}+u\frac{\partial u}{\partial x}\frac{\partial T}{\partial x}+v\frac{\partial v}{\partial r}\frac{\partial T}{\partial r}+v\frac{\partial u}{\partial r}\frac{\partial T}{\partial x}\right]$$
$$=\frac{k}{\rho C_p}\left(\frac{\partial^2 T}{\partial r^2}+\frac{1}{r}\frac{\partial T}{\partial r}\right)+\tau\left[D_B\frac{\partial C}{\partial r}\frac{\partial T}{\partial r}+\frac{D_T}{T_\infty}\left(\frac{\partial T}{\partial r}\right)^2\right], \tag{6}$$

Equation of concentration

$$u\frac{\partial C}{\partial x}+v\frac{\partial C}{\partial r}=D_B\left(\frac{1}{r}\frac{\partial C}{\partial r}+\frac{\partial^2 C}{\partial r^2}\right)+\frac{D_T}{T_\infty}\left(\frac{1}{r}\frac{\partial T}{\partial r}+\frac{\partial^2 T}{\partial r^2}\right), \tag{7}$$

Equation of density of motile germs

$$u\frac{\partial N}{\partial x}+v\frac{\partial N}{\partial r}+\frac{bW_c}{(C_0-C_\infty)}\left[\frac{\partial}{\partial r}\left(N\frac{\partial C}{\partial r}\right)\right]=D_m\left(\frac{\partial^2 N}{\partial r^2}+\frac{1}{r}\frac{\partial N}{\partial r}\right), \tag{8}$$

Subjected to

$$\begin{cases}v=0, \quad k\dfrac{\partial T}{\partial r}=-q_w(x), \quad u=U_w(x), \quad C=C_w, \quad N=N_w & \text{at} r=a,\\ u\to 0, \quad C\to C_\infty, \quad T\to T_\infty, \quad N\to N_\infty & \text{as} r=\infty.\end{cases} \tag{9}$$

In order to achieve the numerical solution of the governing partial differential Eqs. (4)–(8), we make suitable similarity transformations whereby we transform the system into a system of ordinary differential equations.

$$\eta=\frac{r^2-a^2}{2a}\sqrt{\frac{U_0}{\nu l}}, \quad \psi=\sqrt{\nu U_w}af(\eta),$$
$$T=T_\infty+\left(\frac{q_w}{k}\sqrt{\frac{\nu}{U_0}}\right)\theta(\eta), \quad \phi(\eta)=\frac{C-C_\infty}{C_w-C_\infty}, \chi(\eta)=\frac{N-N_\infty}{N_w-N_\infty}. \tag{10}$$

The resultant ODEs are labelled as:

$$(1+2\eta\gamma)f'''+2\gamma\eta f''+(1+\lambda_1)\left(ff''-(f')^2\right)+\beta(1+2\eta\gamma)\left((f'')^2-ff''''\right)$$
$$+\gamma\beta(f'f''-3f'''')-M^2(1+\lambda_1)f'+\overset{*}{\lambda}(\theta-Nr\phi-Nc\chi)$$
$$=0, \tag{11}$$

$$\left(1+2\eta\gamma-\Pr\lambda f^2\right)\theta''+2\gamma\theta'+(1+2\eta\gamma)\left(N_b\theta'\phi'+N_t(\theta')^2\right)$$
$$-Pr\left(f'\theta-f\theta'+\lambda\left(f'^2\theta-ff'\theta'-ff''\theta\right)\right)$$
$$=0, \tag{12}$$

$$(1+2\eta\gamma)\phi''+2\gamma\phi'+\left(\frac{N_t}{N_b}\right)(2\gamma\theta'+(1+2\eta\gamma)\theta'')+LePr(f\phi')=0, \tag{13}$$

$$(1+2\gamma\eta)\chi''+[2\gamma+Lbf]\chi'-Pe[\chi'\phi'+(\chi+\Omega)\phi'']=0. \tag{14}$$

Subjected to

$$\begin{vmatrix}f(\eta)=0, & f'(\eta)=1, & \theta'(\eta)=-1, & \phi(\eta)=1,\chi(\eta)=1, & \eta\to 0,\\ f'(\infty)=0, & \theta(\infty)=0, & \phi(\infty)=0,\chi(\infty)=0 & & \eta\to\infty.\end{vmatrix} \tag{15}$$

The controlling parameters are defined as:

$$\lambda=\frac{\lambda_2 U_0}{l}, \quad M^2=\frac{\sigma B_0^2}{\rho U_0}, \quad \gamma=\sqrt{\frac{l\nu}{a^2U_0}}, \quad Pr=\frac{\nu}{\alpha}, \quad Le=\frac{\alpha}{D_B}, \quad N_b=\frac{\tau D_B(C_w-C_\infty)}{\nu},$$
$$Lb=\frac{\nu}{D_m}, \quad N_r=\frac{(\rho_p-\rho_f)(C_w-C_\infty)}{\rho_f(1-C_\infty)(T_w-T_\infty)\beta}, \quad \lambda_E=\frac{\lambda_E U_0}{l}, \quad \Omega=\frac{N_\infty}{N_w-N_\infty}, \quad Pe=\frac{bW_c}{D_m},$$
$$N_c=\frac{\gamma(\rho_m-\rho_r)(n_w-n_\infty)}{\rho_f(1-C_\infty)(T_w-T_\infty)\beta}, N_t=\frac{\tau D_T(T_w-T_\infty)}{\nu T_\infty}.$$

The engineering quantities are listed as:

$$C_f = \frac{2\tau_w}{\mu U_w^2}, \quad Nu_x = \frac{xq_w}{k(T_w - T_\infty)}, \quad Sh_x = \frac{xq_m}{D_B(C_w - C_\infty)}, \quad Nn_x = \frac{xq_n}{D_n(N_w - N_\infty)}, \tag{16}$$

$$f = y_1, f' = y_2, f'' = y_3, f''' = y_4, \theta = y_5, \theta' = y_6, \phi = y_7, \phi' = y_8, \chi = y_9, \chi' = y_{10}$$

$$\begin{aligned}
&\frac{dy_1}{d\eta} = y_2\\
&\frac{dy_2}{d\eta} = y_3\\
&\frac{dy_3}{d\eta} = y_4\\
&\frac{dy_4}{d\eta} = \frac{1}{(1+2\eta\gamma)y_1 - \lambda y_1^2}\left[-2\gamma y_3 - (1+\lambda_1)\left(y_1 y_3 - y_2^2\right) - \lambda y_3^2 + M^2(1+\lambda_1)y_2 + \overset{*}{\lambda}\left(y_4 - Nry_6 - Ncy_8\right)\right]\\
&\frac{dy_5}{d\eta} = y_6\\
&\frac{dy_6}{d\eta} = \frac{1}{(1+2\eta\gamma) + \lambda_E y_1^2}\left[-2\gamma y_6 - (1+2\eta\gamma)\left(N_b y_6 y_8 + N_t y_6^2\right) - \lambda_E y_1 y_2 y_6 + Pr\left(y_1 y_6 - y_2 y_5\right)\right]\\
&\frac{dy_7}{d\eta} = y_8\\
&\frac{dy_8}{d\eta} = \frac{1}{1+2\eta\gamma}\left[-2\gamma y_8 - \left(\frac{N_t}{N_b}\right)\left(2\gamma y_6 + (1+2\eta\gamma)y_{6'}\right) - LePry_1 y_8\right]\\
&\frac{dy_9}{d\eta} = y_{10}\\
&\frac{dy_{10}}{d\eta} = \frac{1}{1+2\gamma\eta}\left[-(2\gamma + Lby_1)y_{10} + Pe\left(y_{10}y_8 + \left(y_9 + \Omega\right)\frac{dy_8}{d\eta}\right)\right]
\end{aligned} \tag{20}$$

$$\tau_w = \left[\frac{\mu}{(1+\lambda_1)}\left(\frac{\partial u}{\partial r}\right) + \frac{\mu\lambda_2}{(1+\lambda_1)}\left(\frac{\partial^2 u}{\partial r^2} + u\frac{\partial^2 u}{\partial x \partial r}\right)\right]_{r=a,} \tag{17}$$

$$q_w = -k\left(\frac{\partial T}{\partial r}\right)_{r=a}, \quad q_m = -D_B\left(\frac{\partial C}{\partial r}\right)_{r=a}, \quad q_n = -D_m\left(\frac{\partial N}{\partial r}\right)_{r=a,} \tag{18}$$

Dimensionless of engineering quantities are extracted as:

$$\begin{aligned}
&\frac{C_f (Re_x)^{1/2}}{2} = \frac{1}{(1+\lambda_1)}[f''(0) + \lambda(\gamma f'''(0)f'(0) - f'''(0)f'(0) + f''(0)f'(0))],\\
&\frac{Nu_x}{\sqrt{Re_x}} = -\theta(0), \quad \frac{Sh_x}{\sqrt{Re_x}} = -\phi(0), \quad \frac{Nn_x}{\sqrt{Re_x}} = -\chi(0).
\end{aligned} \tag{19}$$

Where $Re_x = \frac{U_w x}{\nu}$.

3. Numerical technique

The resulting set of ODEs is highly nonlinear and intensely coupled, making an exact analytical solution unachievable. To concentrate this, a well-established numerical approach the shooting technique, implemented using bvp4c tool of MATLAB. The procedural stages of the shooting process are outlined below (see Fig. 1c). The shooting method with bvp4c package deals numerous compensations, containing flexibility in solving coupled ODEs, high accuracy and straightforward execution. To confirm solution accurateness, the package was utilized with both relative and absolute error tolerances set to 10^{-6}.

4. Results and discussions

This section presents the numerical findings for bioconvective Jeffrey nanofluid flow over a stretching cylinder under the combined influence of Cattaneo-Christov heat flux and magnetic field. The governing parameters investigated include magnetic number (M), curvature parameter (γ), Jeffrey fluid parameter (β), bioconvective Lewis number (Lb), buoyancy ratio parameter (Nr), relaxation time parameter (λ_1), Prandtl number (Pr), thermal relaxation parameter (λ), thermophoresis parameter (Nt), Lewis number (Le), Brownian motion parameter (Nb), bioconvective Péclet number (Pe), and microorganisms difference parameter (Ω). Their effects on velocity, temperature, concentration, microorganism density profiles, and engineering quantities are illustrated in Figs. 2–22.

5. Velocity field analysis

Fig. 2(a-b) shows the reaction of velocity distribution $f(\eta)$ to the change in the magnetic parameter ($M = 0.2, 0.6, 1.2, 1.7, 2.2$). The forces of Lorentz are created as a result of the application of transverse magnetic field and act against the movement of the fluid. These resistive forces are intensified as M increases between 0.2 and 2.2 resulting in a gradual attenuation of the velocity. At $M = 0.2$ the maximum is reached and at $M = 2.2$ the minimum. The cause of this effect of retarding is due to the fact that the magnetic field tends to align the particles in the non-Newtonian fluids hence enhancing the resistance to flow in the boundary layer. The velocity increase with curving parameter ($\gamma = 0.0, 0.2, 0.4, 0.6, 0.8$) is depicted in Fig. 3(a-b). The increased γ values will

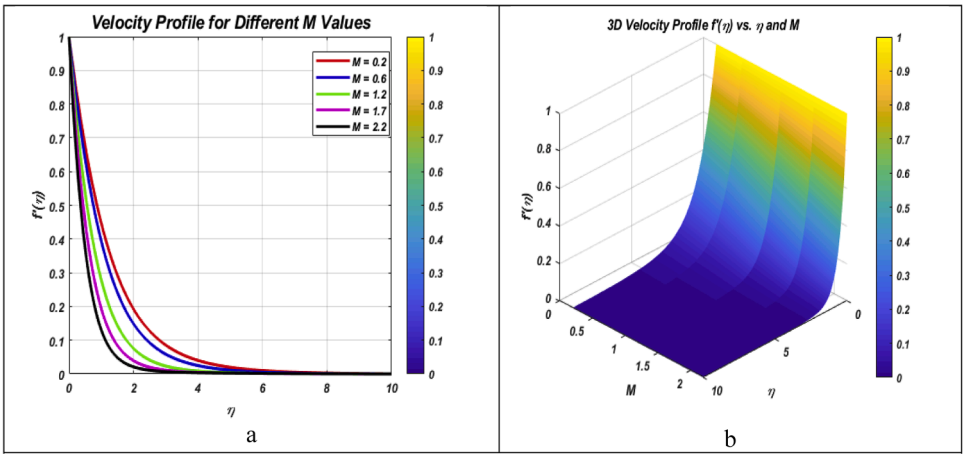

Fig. 2. (a-b). Influence of magnetic number M (=0.2, 0.6, 1.2, 1.7, 2.2) on velocity profile.

indicate a smaller cylinder radius, which will increase the effect of stretching pressure and speed up fluid flow. The maximum velocity profile is reached at $\gamma = 0.8$ of gamma and the minimum at the case of a flat plate ($\gamma = 0.0$). This is due to the fact that in the curved geometries, transfer of momentum is enabled since there is a greater exposure of surface area per unit volume. Fig. 4(a-b) shows the impact of the Jeffrey parameter (β) on velocity distribution. Systematic β increase of lower to higher value decreases the velocity of fluids. This reduction is possible since high (β) increases the resistance of fluid to deformation due to increased effects of relaxation. The viscoelastic properties of the material predominate and increase the delay of the fluid response to the applied stress and, therefore, reduce the flow velocity. Fig. 5(a-b) shows that velocity profiles are suppressed with increase in buoyancy ratio parameter (Nr). An increase in Nr leads to a stronger solutal buoyancy

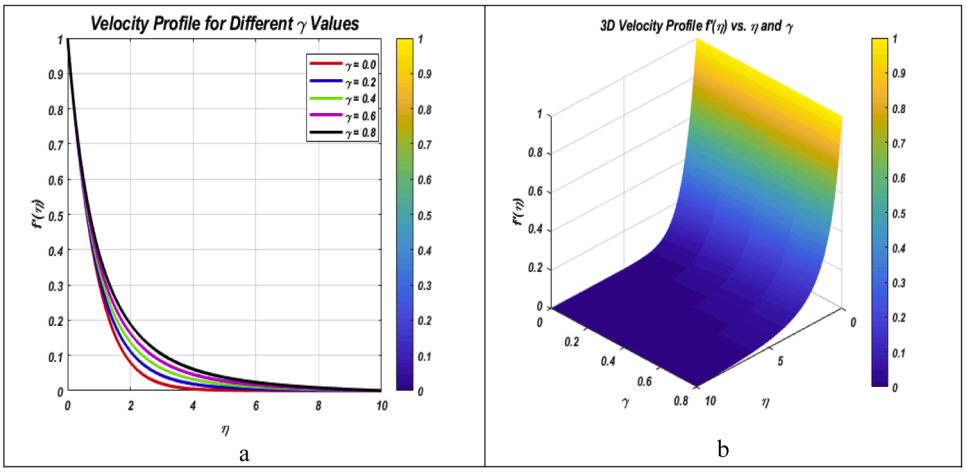

Fig. 3. (a-b). Influence of curvature parameter γ (=0.0, 0.2, 0.4, 0.6, 0.8) on velocity profile.

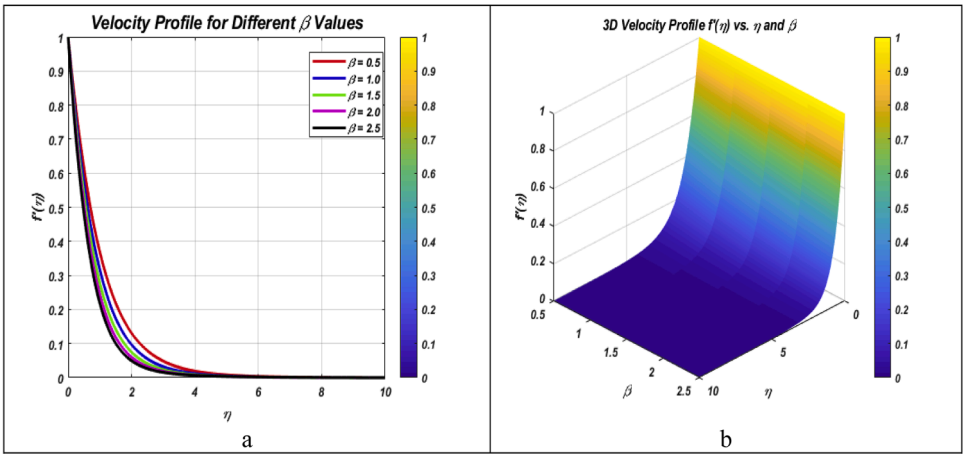

Fig. 4. (a-b). Influence of Jeffrey fluid β(=0.5, 1.0, 1.5, 2.0, 2.5) on velocity profile.

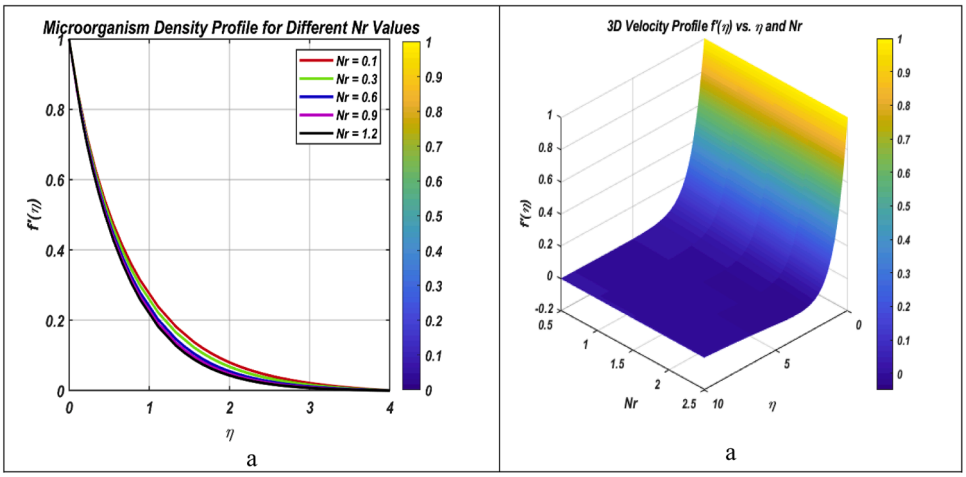

Fig. 5. (a-b). Influence of buoyancy ratio parameter *Nr* (=0.5, 1.0, 1.5, 2.0, 2.5) on velocity profile.

force in comparison with thermal buoyancy force in the channel and breaks the momentum equilibrium of the flow field. This disequilibrium lowers the net driving force of the fluid motion and this causes a decrease in velocity over the boundary layer. Fig. 6(a-b) illustrates the velocity response to the changes in relaxation time parameter (λ_1). Increased λ_1 values translate to longer relaxation times of stress, in other words the fluid takes long before it can adjust to deformation. This sluggish mechanical reaction is associated with sluggish flow rates and, therefore, decreased velocity distributions across the domain.

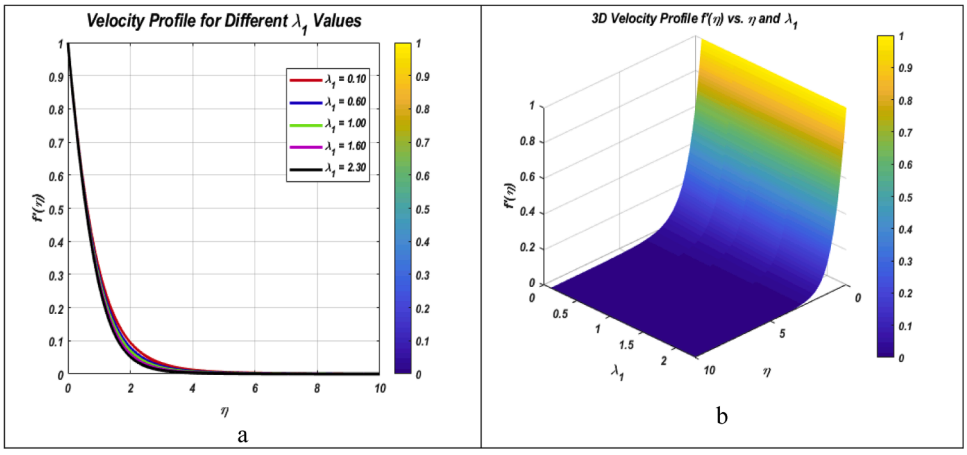

Fig. 6. (a-b). Influence of relaxation time parameter λ_1(=0.10, 0.60, 1.00, 1.60, 2.30) on velocity profile.

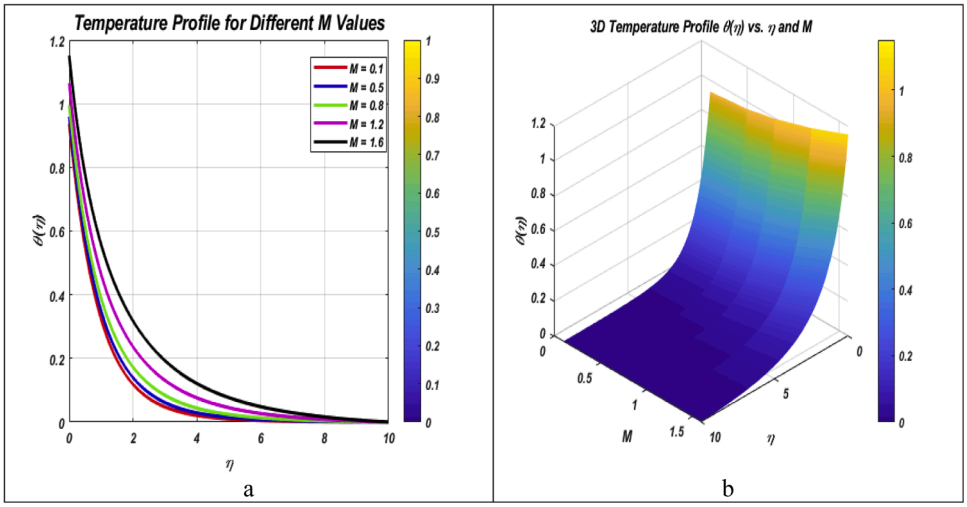

Fig. 7. (a-b). Influence of magnetic number *M* (=0.1, 0.5, 0.8, 1.2, 1.6) on temperature profile.

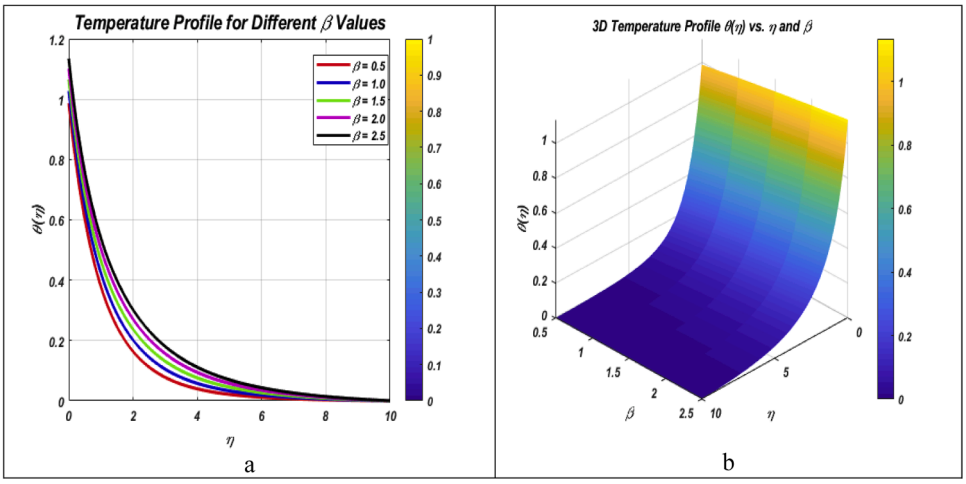

Fig. 8. (a-b). Influence of Jeffrey fluid β(=0.5, 1.0, 1.5, 2.0, 2.5) on temperature profile.

6. Temperature field analysis

Fig. 7(a-b) represents temperature profiles of magnetic parameter values ($M = 0.1, 0.5, 0.8, 1.2, 1.6$). Continuous incremental changes in M raise the temperature distribution. This heating is caused by Joule heating (resistive heating) that is co-located with the Lorentz force. The higher the strength of the magnetic field, the larger is the portion of electromagnetic energy that turns into thermal energy in the fluid, increasing the temperature of the fluid. It is seen in Fig. 8(a-b), the thermal behavior of modifications in the Jeffrey parameters. The

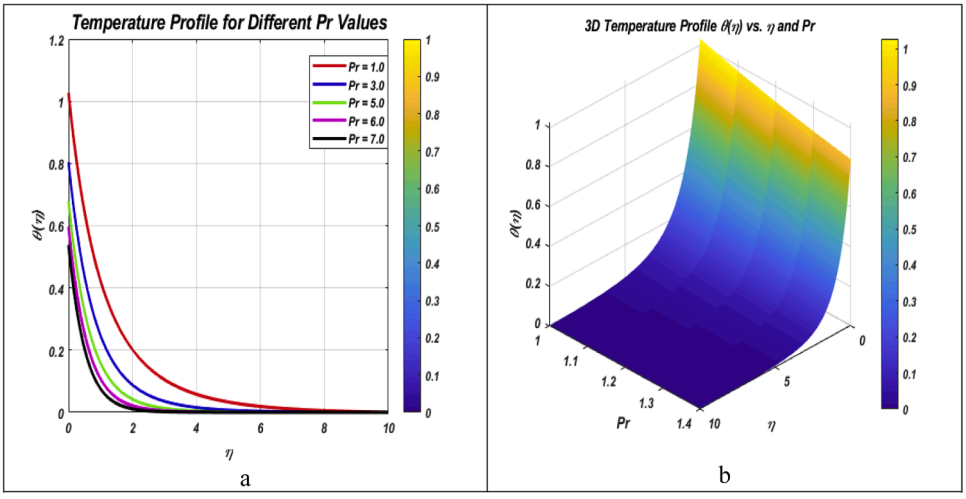

Fig. 9. (a-b). Influence of Prandtl number Pr (=1.0, 3.0, 5.0, 6.0, 7.0) on temperature profile.

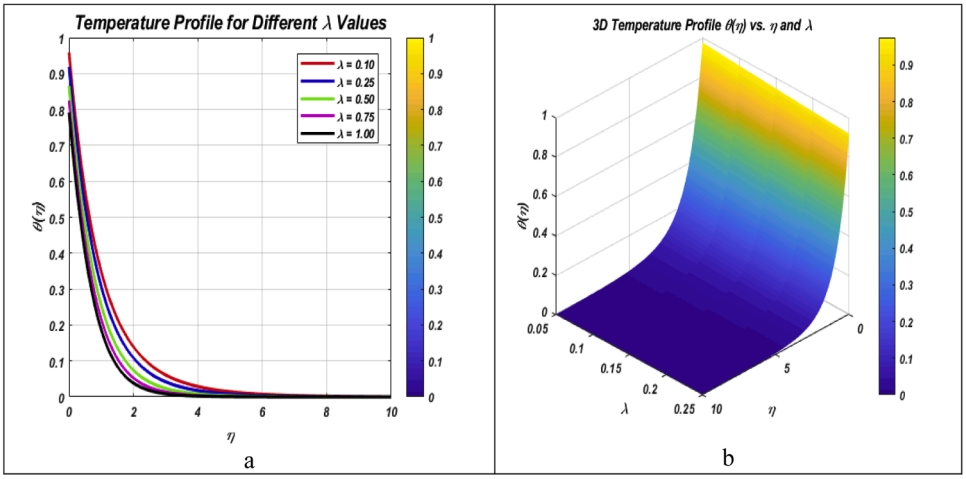

Fig. 10. (a-b). Influence of thermal relaxation parameters λ (=0.10, 0.25, 0.50, 0.75, 1.00) on temperature profile.

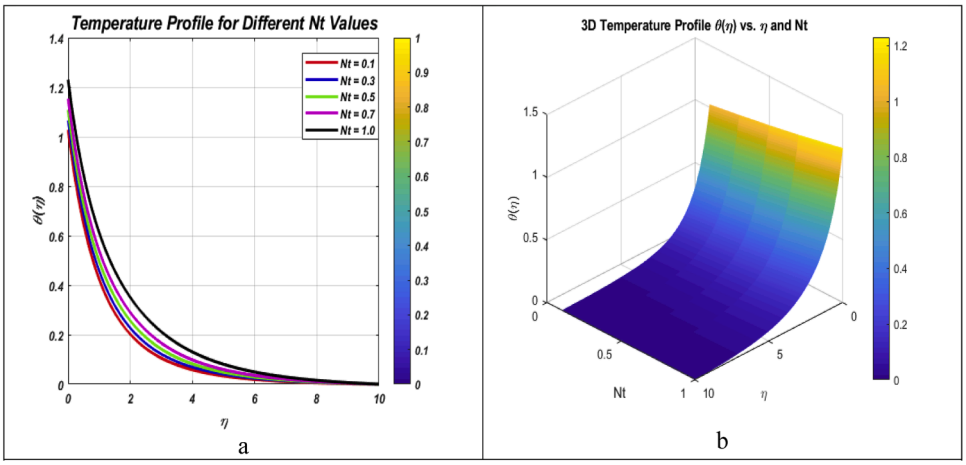

Fig. 11. (a-b). Influence of thermophoresis *Nt* (=0.1, 0.3, 0.5, 0.7, 1.0) on temperature profile.

increase in β values encourages the increase in temperature across the boundary layer. This thermal gain is indicative of altered heat transport properties of the Jeffrey fluids in which due to the viscoelastic nature the thermal diffusion mechanisms are different than that of Newtonian fluids. Fig. 9(a-b) demonstrates temperature curves of different Prandtl numbers. The systematic increase in *Pr* decreases the temperature field. This negative correlation is due to the fact that *Pr* is defined by the ratio between momentum diffusivity and thermal diffusivity. An increase in *Pr* values means a decrease in thermal diffusivity, which limits the penetration of heat into the fluid. This phenomenon has practical

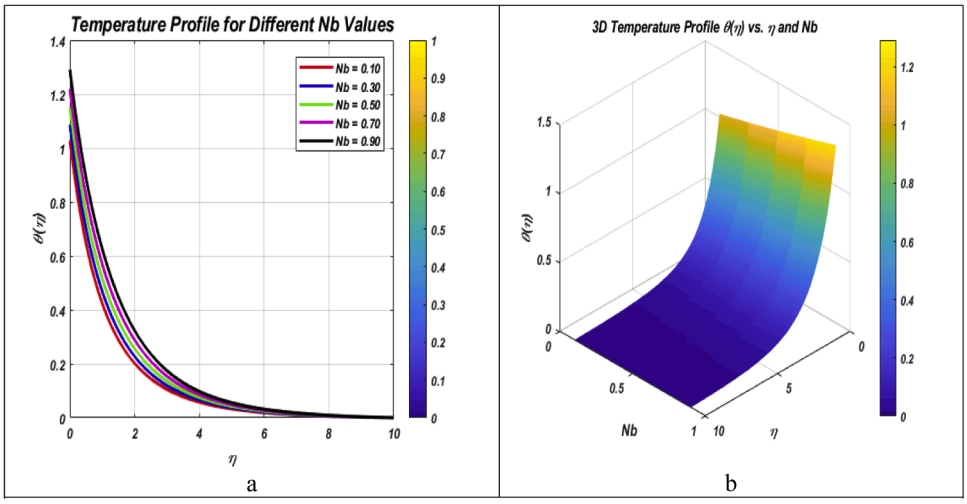

Fig. 12. (a-b). Influence of Brownian motion *Nb* (=0.10, 0.30, 0.50, 0.70, 0.90) on temperature profile.

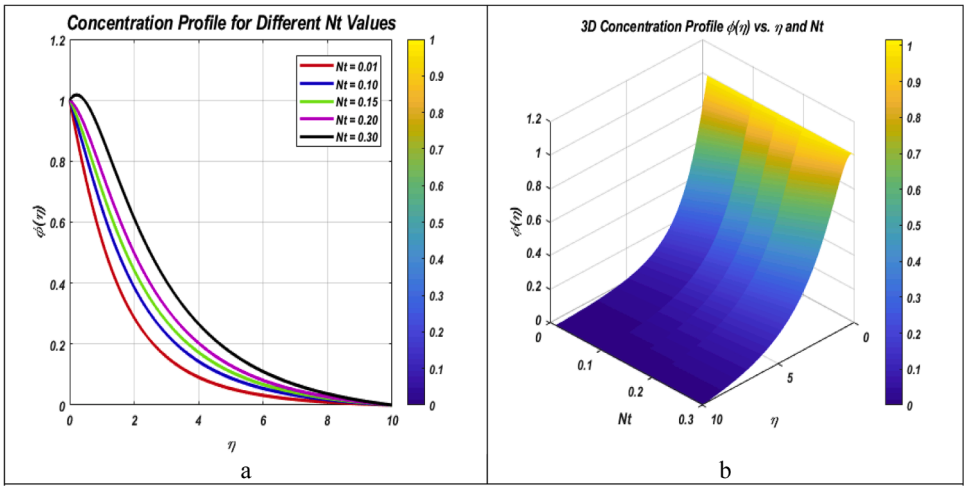

Fig. 13. (a-b). Influence of thermophoresis *Nt* (=0.01, 0.10, 0.15, 0.20, 0.30) on concentration profile.

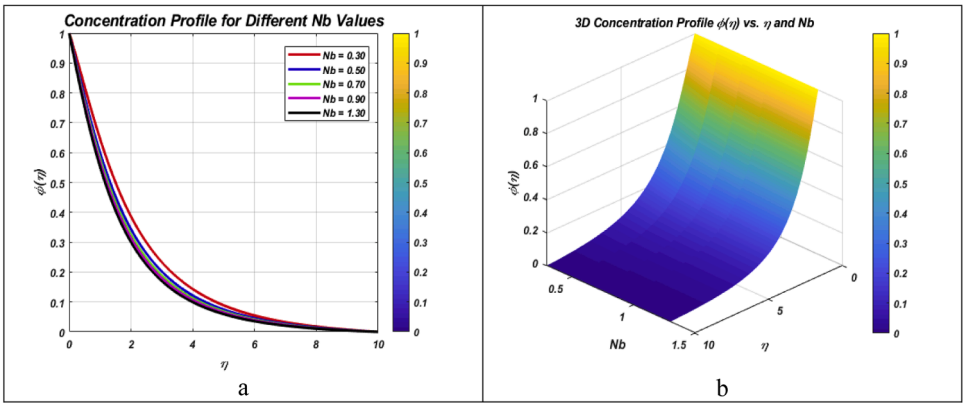

Fig. 14. (a-b). Influence of Brownian motion *Nb* (=0.30, 0.50, 0.70, 0.90, 1.30) on concentration profile.

implications to the high-Prandtl-number fluids such as oils and lubricants, in which thermal insulation must be maintained by control of heat transmission. Fig. 10(a-b) illustrates the suppressing effect of the thermal relaxation parameter (λ) on temperature. Increasing λ results in a significant drop in temperature profiles. Physically, the large λ is an indication of slow thermal conduction, when the particles of the fluid take a long time to move thermal energy to the adjacent areas.

This slowness in the conduction of heat, minimizes the total temperature obtained in the boundary layer. Fig. 11(a-b) suggests the temperature response to the changes of thermophoresis parameters ($Nt = 0.1, 0.3, 0.5, 0.7, 1.0$). Increased values of *Nt* increase temperature distributions significantly. The forces of thermoprotection cause nanoparticles to move in warmer to cooler areas, and moves promote energy transfer in addition to thermal energy accumulation in distinct areas. Fig. 12(a-b) indicates the increment in temperatures with the increment of Brownian motion parameter ($Nb = 0.10, 0.30, 0.50, 0.70, 0.90$). Enhanced Brownian motion leads to stronger random motion of nanoparticles, which enhances dispersion and mixing. This increased the interaction between particles and hence the thermal energy distribution becomes more effective giving higher and smoother temperature profiles in the fluid.

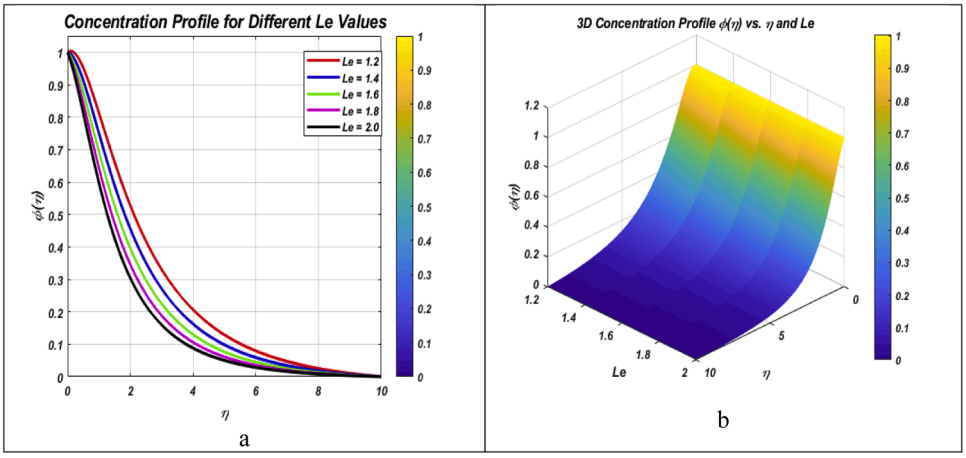

Fig. 15. (a-b). Influence of Lewis number *Le* (=1.2, 1.4, 1.6, 1.8, 2.0) on concentration profile.

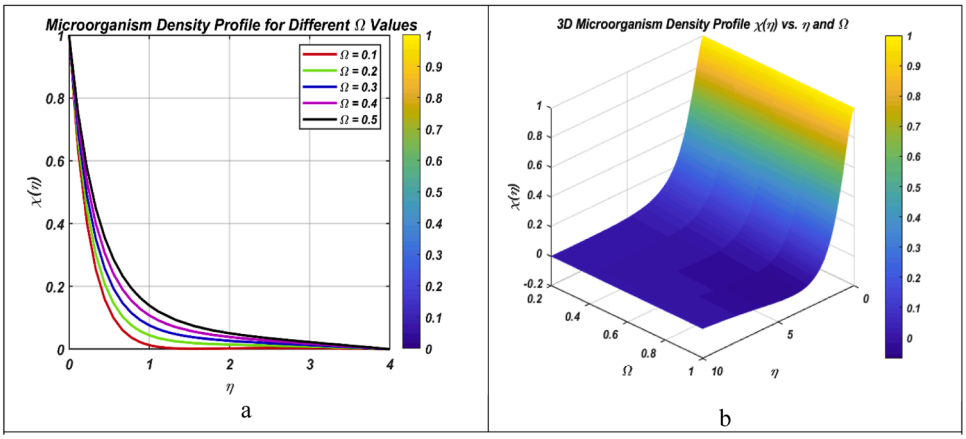

Fig. 16. (a-b). Influence of microorganisms difference parameter Ω (=0.2, 0.4, 0.6, 0.8, 1.0) on microorganisms density profile.

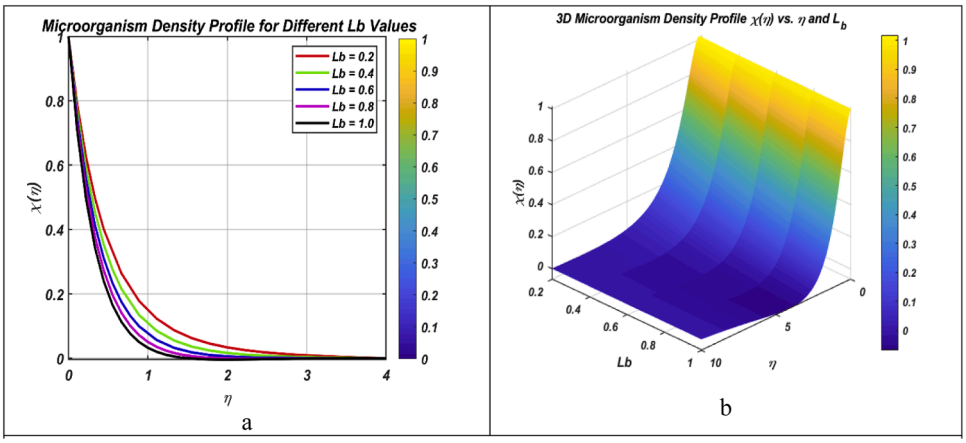

Fig. 17. (a-b). Influence of bioconvective Lewis number *Lb* (=0.2, 0.4, 0.6, 0.8, 1.0) on microorganisms density profile.

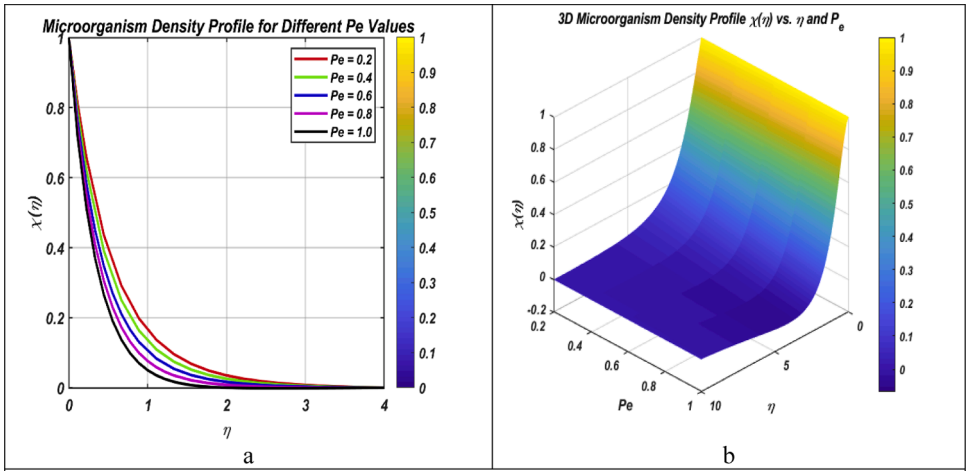

Fig. 18. (a-b). Influence of bioconvective Peclet number *Pe* (=0.2, 0.4, 0.6, 0.8, 1.0) on microorganisms density profile.

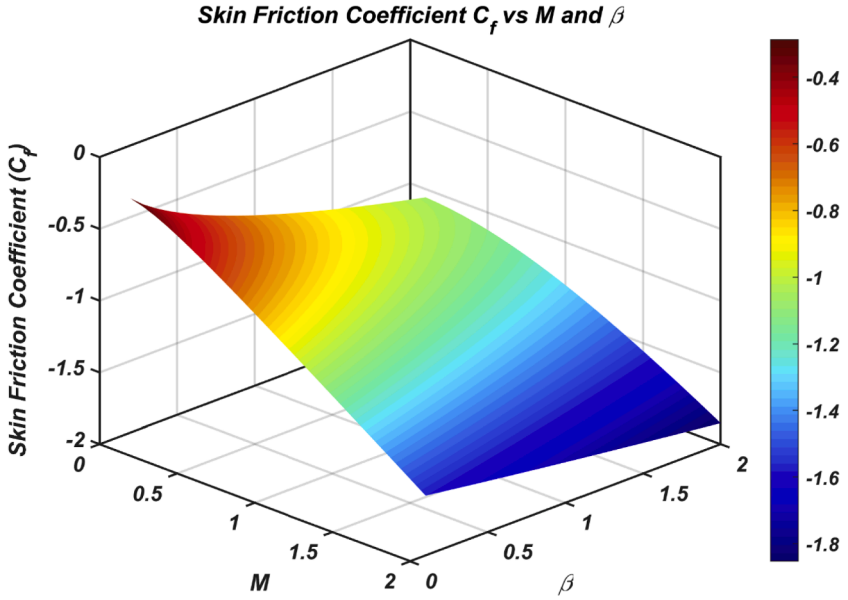

Fig. 19. Plot of Skin Friction C_f and M vs β.

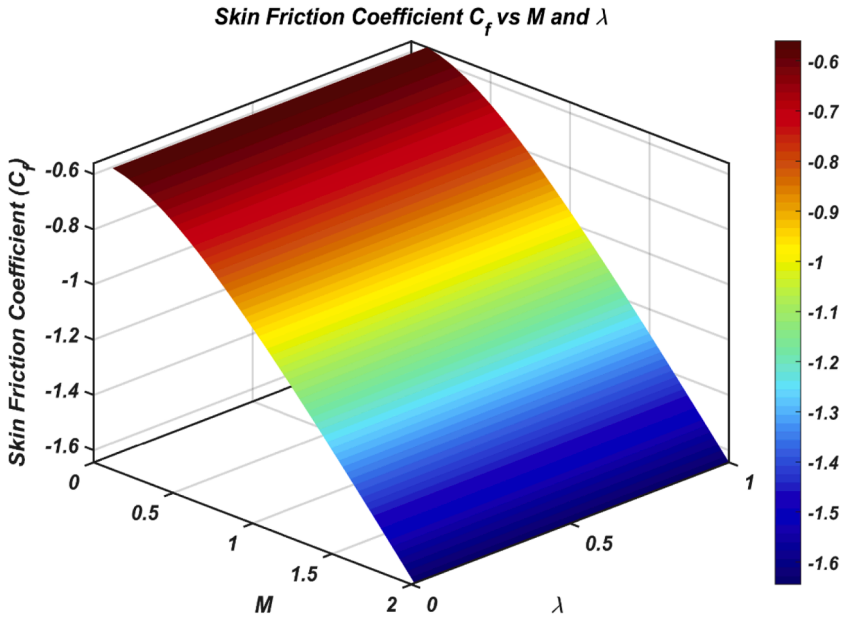

Fig. 20. Plot of Skin Friction C_f and M vs λ.

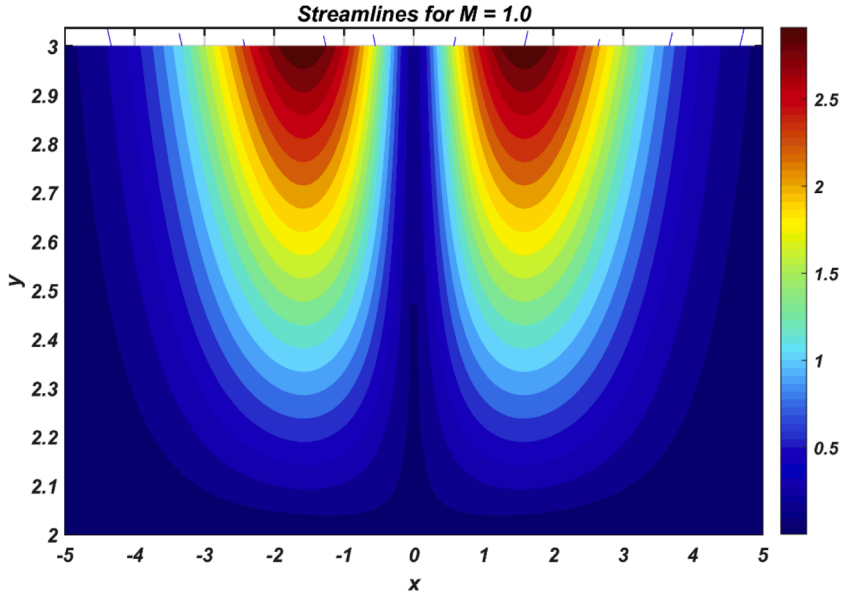

Fig. 21. Streamline pattern for $M = 1.0$.

7. Concentration field analysis

Fig. 13(a-b) shows concentration profiles of changes in the thermophoresis parameters ($Nt = 0.01, 0.10, 0.15, 0.20, 0.30$). An increment in Nt values increases the concentration field ϕ progressively. This is due to the fact that the stronger the thermophoretic forces the higher the concentration of nanoparticles will be brought towards the hotter surface by the cooler regions and hence the greater the concentration of nanoparticles at the boundary. The behavior response to variations of Brownian motion in the concentration field is illustrated in Fig. 14(a-b). Contrary to the effect of Brownian motion on temperature, with more Brownian motion, concentration profiles get smaller. This decrease is caused by increased random particle movement and increased collisions, dispersing nanoparticles and homogenizing the distribution of concentration, decreasing concentrate accumulation. Fig. 15(a-b) illustrations the consequence of the Lewis number ($Le = 1.2, 1.4, 1.6, 1.8, 2.0$) on concentration field. Concentration profiles are diminishing in a systematically manner as Le increases. Given that Lewis number is directly proportional to mass diffusivity, the bigger the mass diffusion capacity, the smaller the Lewis number. This reduced diffusive transport will reduce nanoparticle dispersion, and their concentration will be low in the boundary layer.

8. Microorganism density field analysis

As shown in Fig. 16(a-b), it can be seen that the density of microorganisms χ is responsive to changes in the microorganism difference parameter ($\Omega = 0.2, 0.4, 0.6, 0.8, 1.0$). The density of swimming microorganisms decreases with the increasing of Ω. This parameter controls the spatial distribution of motile microorganisms with significant consequences in regard to optimization of bioconvection processes in bioengineering applications of microbial suspensions. Fig. 17(a-b)

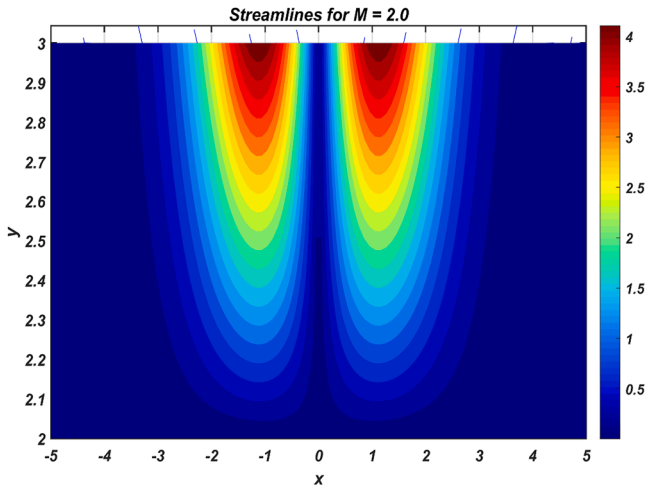

Fig. 22. Streamline pattern for $M = 2.0$.

Table 1
The numerical comparison of current outcomes with those reported in the existing literature when when $Nt = M = Nb = \lambda = Lb = Pe = \lambda_1 = Pe = \gamma = \beta = \Omega = 0$.

Nu		
Pr	[42]	Present
0.72	1.2314	1.2314
1.0	0.9995	0.9995
6.7	0.3333	0.3333
10	0.2687	0.2687

Table 2
Effect of fluid parameters on Skin friction coefficient C_f.

	M	*Nr*	*Nc*	C_f
0.1				-1.05031
0.5				-0.88279
1.0				-0.75617
	0.1			-1.01860
	0.5			-1.12325
	1.0			-1.40795
		0.1		-1.59806
		0.2		-1.62906
		0.3		-1.66944
			0.1	-1.59832
			0.2	-1.59806
			0.3	-1.63429

Table 3
Effect of fluid parameters on Nusselt number *Nu*.

	M	λ	*Nt*	*Nb*	*Nu*
0.1					1.23780
0.5					1.21388
1.0					1.18893
	0.1				1.21388
	0.5				1.19570
	1.0				1.15009
		0.1			1.09480
		0.5			1.30856
		1.0			1.49630
			0.05		1.23378
			0.1		1.21388
			0.2		1.16564
				0.05	1.28504
				0.1	1.21388
				0.2	1.15064

Table 4
Effect of fluid parameters on Sherwood number *Sh*.

λ	*M*	γ	*Le*	β	*Sh*
0.1					2.76090
0.5					2.74942
1.0					2.73045
	0.1				2.23189
	0.5				2.23047
	1.0				2.21891
		0.1			1.64943
		0.5			2.23047
		1.0			2.75454
			0.5		2.07520
			1.0		2.23047
			2.0		2.45588
				0.3	2.22788
				0.5	2.23047
				0.7	2.23259

Table 5
Effect of fluid parameters on motile microorganism density number *Nn*.

λ	*M*	*Pe*	*Lb*	Ω	*Nn*
0.1					1.89503
0.5					1.89808
1.0					1.89506
	0.1				1.89820
	0.5				1.89191
	1.0				1.87499
		0.1			0.82907
		0.5			1.89820
		1.0			3.28704
			0.1		1.79031
			0.5		1.89820
			1.0		2.03433
				0.05	1.83863
				0.1	1.89820
				0.2	2.01736

shows how density of microorganisms is affected by bioconvection Lewis number (*Lb*). An increase in *Lb* values inhibits the microorganism density profile χ. This decrease suggests that high bioconvection Lewis numbers restrict the growth of microbes, which is a control system of bioconvection where toxin systems with microbes. Fig. 18(a-b) indicates density response of microorganisms to changes in Peclet number (*Pe*). The growing *Pe* declines the density distribution χ, which is indicative of developed advective transport that disperses microorganisms further throughout the domain. Such behavior is practically important in the application of environmental engineering and bioreactor design, where the distribution of microbes has to be controlled.

9. Surface drag and transport characteristics

Figs. 19 and 20 show the joint influence of magnetic parameter (*M*), Jeffrey fluid parameter (β), and thermal relaxation parameter (λ) on skin friction coefficient C_f. The introduction of magnetic fields creates the Loriors forces which alter the near-surface shear distribution. The Jeffrey parameter β, reflects the viscoelastic properties of the fluid, and it dictates the equilibrium between the viscous and elastic responses. In the meantime, the relaxation parameter λ is the delayed deformation response of the fluid and it varies the transport of momentum in the boundary layer. The patterns of streamlines of the magnetic parameters, $M = 1.0$ and $M = 2.0$, are compared in the Figs. 21 and 22. The magnetic field has a significant effect on flow structure due to the generation of Lorentz forces that change curvature of the streamlines and inhibit flow in the fluid in the vicinity of the cylindrical surface. The effect is a magnetic field that offers a process of flow control through which fluid transport is to be controlled.

10. Validation and quantitative results

Table 1 provides numerical comparison of the current investigation and the literature available in the past. The great agreement proves the correctness and credibility of the current methodology of computations. The influence on the engineering quantities, i.e. skin friction coefficient (C_f), Nusselt number (Nu), Sherwood number (Sh) and the density number of motile microorganisms (Nn) of various fluid parameters were documented in Tables 2–5. These tabulated data are used to give quantitative values of the heat transfer, mass transfer, and microbial transport properties of the mixture of magnetic field, Cattaneo-Christov heat flux, and Jeffrey fluid properties.

11. Conclusion

This paper involves numerical research on two-dimensional electromagnetic flow of Jeffrey nanofluid over an extending cylinder and includes Cattaneo-Christov heating flux, bioconvection processes, Brownian diffusion, thermophoresis, and motile microorganisms. The discussion of the effects of these coupled processes on velocity, thermal, concentration and microorganism density distributions and the engineering parameters of skin friction, heat transfer rate, mass transfer rate and motile microorganism flux is done. The main conclusions that were made out of this investigation are as follows:

- The velocity profile shows a systematic decrease with increasing values of the Jeffrey fluid parameter β, magnetic parameter M and bioconvection Rayleigh number Nr. The interaction of the retarding effects of the viscoelastic properties and Lorentz force with that of buoyancy validate this behavior. Interestingly, a negative dependence is found between the magnitudes of velocity and the curvature parameter which means that the development of the boundary layers is large scale, and cylinder curvature causes it to vary.
- There is a significant increase in temperature distribution as the thermophoresis parameter Nt, magnetic parameter M and Brownian motion parameter Nb increases. This is attributed to enhanced thermal energy transfer processes, such as thermophoretic particle movement, Joule heating due to the magnetic field interaction, and enhanced dissemination of nanoparticles by random movement. On the other hand, the rise in the thermal relaxation parameter λ and Prandtl number Pr hinders elevation in temperature, which proves the crucial factors of thermal inertia and lower thermal diffusivity in the process of heat transfer control.
- Nanoparticle concentration field steadily decreases with increasing thermophoresis parameter Nt, Lewis number Le and Brownian number Nb. This behavior is indicative of outward diffusion of particles by thermophoretic forces, decreasing mass diffusivity with an increase in the Lewis number, and increased dispersion of particles by Brownian agitation, all of which lead to the decreased accumulation of localized concentration.
- The density of the motile microorganisms decreases significantly as Peclet number Pe, microorganism difference parameter, Omega, and bioconvective Lewis number Lb, increase. This decrease points out to lower bioconvective transport at higher conditions of increased motile activity, concentration gradient of high microbial levels, and increased diffusive resistance of the suspension.
- Streamlining In visualizing, it is found that application of magnetic fields fundamentally changes flow topology in the vicinity of the cylindrical surface. The effectiveness of the electromagnetic control is evident in the effectiveness of the electromagnetic fields to regulate fluid flow in bioconvective systems because stronger magnetic fields result in more pronounced flow inhibition and altered circulation patterns.

These results form part of the realization of understanding complex transport in bioconvective Jeffrey nanofluid system that has possible applications in advanced cooling systems, microbial fuel cells and biomedical devices in which coordinated heat, mass and microorganism transport is vital.

12. Future research

This work can be extended by investigating the influence of various non-Newtonian fluids, different base fluids, a range of nanoparticles, and alternative geometries.

13. Applications

- Biomedical engineering: Understanding the flow of Jeffrey-type fluids with motile microorganisms can aid in drug delivery, biofluid transport and biological processes
- Industrial cooling systems: The results are useful for optimizing heat and mass transfer in wire-drawing system. polymer coating and extrusion.
- Energy and thermal management: The study provides insights for improving the efficiency of energy storage devices, solar collectors and heat exchangers, electromagnetics nanofluids.
- Environmental and bioconvective processes: The analysis helps in predicting microorganism behavior in natural convection processes, wastewater treatment and bioreactors.

Nomenclature		
Wall heat flux	W/m^2	q_w
Brownian motion parameter	m^2/s	Nb
Brownian diffusion coefficient		D_B
Thermophoresis parameter		Nt
Curvature parameter		γ
Thermophoresis diffusion coefficient	m^2/s	D_T
Bio convection Lewis number		Lb
Cell swimming speed	m/s	W_c
Peclet number		Pe
Magnetic parameter		M
Ambient temperature	K	T_∞
Temperature	K	T
Applied magnetic field	T (tesla)	B_0
Direction normal to surface		r
Density of fluid	kg/m^3	ρ
Kinematic viscosity	m^2/s	υ
Radius of cylinder	m	R
Velocity components	m/s	(u, v)

CRediT authorship contribution statement

Muhammad Jawad: Writing – review & editing, Writing – original draft, Validation, Software, Methodology, Investigation, Conceptualization. **Ali B.M. Ali:** Methodology, Formal analysis. **Aaqib Majeed:** Supervision, Data curation. **Narinderjit Singh Sawaran Singh:** Validation, Resources. **Abdul Kareem Abdul Jawwad:** Writing – review & editing, Visualization, Investigation. **Hakim AL Garalleh:** Resources, Investigation, Data curation. **Ibrahim Mahariq:** Writing – review & editing, Resources.

Declaration of competing interest

The authors declare that they have no known competing financial interests or personal relationships that could have appeared to influence the work reported in this paper.

Data availability

Data will be made available on request.

References

[1] S.U. Choi, J.A. Eastman, Enhancing Thermal Conductivity of Fluids with Nanoparticles, Argonne National Lab.(ANL), Argonne, IL (United States), 1995,

https://doi.org/10.1115/IMECE1995-0926 (No. ANL/MSD/CP-84938; CONF-951135-29).
[2] S.M. Vahidhosseini, M.A. Bidi, S. Rashidi, Thermophysical properties of magnetic nanofluids under effects of magnetic field-a review on mechanisms and studies, J. Therm. Anal. Calorim. (2024) 1–36, https://doi.org/10.1007/s10973-024-13490-0.
[3] H. Upreti, S.R. Mishra, A.K. Pandey, P. Bartwal, Shape factor analysis in stagnation point flow of casson nanofluid over a stretching/shrinking sheet using Cattaneo–Christov model, Numer. Heat Transf. B: Fundam. 85 (10) (2024) 1381–1397, https://doi.org/10.1080/10407790.2023.2265555.
[4] S. Sahamifar, D. Naylor, T. Yousefi, J. Friedman, Measurement of the thermal conductivity of nanofluids using a comparative interferometric method, Int. J. Therm. Sci. 199 (2024) 108890, https://doi.org/10.1016/j.ijthermalsci.2024.108890.
[5] Y. Akbar, S. Huang, A. Magesh, J. Ji, M.M. Alam, Thermal analysis of mixed convective peristaltic pumping of nanofluids in the occurrence of an induced magnetic field and variable viscosity, J. Taibah Univ. Sci. 18 (1) (2024) 2319890, https://doi.org/10.1080/16583655.2024.2319890.
[6] U. Farooq, A. Basem, M. Imran, N. Fatima, M. Tahir, H. Waqas, A. Ibrahim, Numerical computational of chemically reactive hybrid nanofluids with melting phenomena passing through a disk: comparative study, J. Nanofluids 13 (3) (2024) 831–838, https://doi.org/10.1166/jon.2024.2167.
[7] W.H. Hassan, M.D. Kumar, K. Govindarajulu, N.S.S. Singh, M. Jawad, W. Abdelfattah, H.A. Garalleh, Thermal assessment of Maxwell–Sutterby fluid with bio-convection and activation energy effects induced by Riga plate via Levenberg–Marquardt algorithm, Results Eng. (2025) 105819, https://doi.org/10.1016/j.rineng.2025.105819.
[8] U. Farooq, A. Basem, S.A. Khan, N. Fatima, H. Liu, M. Imran, T. Muhammad, Melting hydrothermal analysis of MHD hybrid–Based nanomaterials (SWCNTS-MWCNT/EG-Water) flow driven by double stretchable rotating disks, BioNanoScience 14 (3) (2024) 2509–2528, https://doi.org/10.1007/s12668-024-01468-z.
[9] Y. Aboel-Magd, A. Basem, U. Farooq, N. Fatima, S. Noreen, H. Waqas, M. Iftikhar, Computational modeling of thermal radiation and activation energy effects in Casson nanofluid flow with bioconvection and microorganisms over a disk, Int. J. Thermofluids 23 (2024) 100735, https://doi.org/10.1016/j.ijft.2024.100735.
[10] M. Waseem, I. Omar, M. Jawad, T. Saidani, Q.M. Al-Mdallal, Impact of Cattaneo-Christov heat and surface temperature on viscoelastic non-newtonian micropolar nanofluids: Darcy exponential sheet flow with planktonic microorganisms, Int. J. Thermofluids 26 (2025) 101131, https://doi.org/10.1016/j.ijft.2025.101131.
[11] N. Bahman, Z. Abbas, M.S. Arslan, M.Y. Rafiq, Exploring entropy production in radiative cilia flow of Williamson fluid through a curved channel with viscous dissipation effects, J. Radiat. Res. Appl. Sci. 18 (2) (2025) 101566, https://doi.org/10.1016/j.jrras.2025.101566.
[12] T. Salahuddin, A. Maqsood, M. Awais, M. Khan, M. Afzal, Heat generation of Cross fluid model over a stretching sheet with chemical reaction, Geoenergy Sci. Eng. (2025) 213989, https://doi.org/10.1016/j.geoen.2025.213989.
[13] E.A. Algehyne, F.M. Alamrani, I. Haq, M.M. Seada, S.A. Lone, A. Saeed, A numerical analysis of three-dimensional MHD convective flow of Maxwell nanofluids over an extending surface with Cattaneo–Christov heat and mass flux, Multiscale Multidiscip. Model. Exp. Des. 8 (3) (2025) 193, https://doi.org/10.1007/s41939-025-00778-3.
[14] M. Dehghan Afifi, A. Jahangiri, M. Ameri, Numerical and analytical investigation of jeffrey nanofluid convective flow in magnetic field by FEM and AGM, Int. J. Thermofluids 25 (2025) 100999, https://doi.org/10.1016/j.ijft.2024.100999.
[15] P. Devi, G.C. Rana, S.R. Sharma, S. Kumar, P.K. Gautam, Impact of rotation on thermal instability of Darcy–Brinkman porous layer filled with a Jeffrey nanofluid, Numer. Heat Transf. A: Appl. 86 (6) (2025) 1419–1434, https://doi.org/10.1080/10407782.2023.2273456.
[16] A. Alameer, A. Eladeb, H.F.M. Ameen, N. Fatima, M. Abbas, Y. Khan, A.M. Galal, Estimation of induction effects on electrophoresis and thermophoresis particles deposition in radiative flow of trihybrid nanofluid across cylinder, J. Radiat. Res. Appl. Sci. 18 (1) (2025) 101222, https://doi.org/10.1016/j.jrras.2024.101222.
[17] R.H. Hameed, R.A. Hussein, Q.H. Al-Salami, M.A. Alomari, A.M. Hassan, F. Q. Alyousuf, M.A. Flayyih, Free convection investigation for a Casson-based Cu–H2O nanofluid in semi parabolic enclosure with corrugated cylinder, Heliyon 11 (1) (2025), https://doi.org/10.1016/j.heliyon.2025.e42558.
[18] V. Puneeth, K. Sini, T. Clair, M.S. Anwar, Flow of nanofluid past a stretching cylinder subject to Thompson and Troian slip in the presence of gyrotactic microorganisms, Multiscale Multidiscip. Model. Exp. Des. 8 (1) (2025) 84, https://doi.org/10.1007/s41939-024-00667-1.
[19] A. B.R. Sreenivasa, J. Faqeeh, A. Alsaiari, H.A. Alzahrani, M.Y. Malik, Numerical study of heat transfer mechanism in the flow of ferromagnetic hybrid nanofluid over a stretching cylinder Waves Random Complex Media 35 (3) (2025) 4339–4355, https://doi.org/10.1080/17455030.2022.2061084.
[20] S. Munir, Y.U.U.B. Turabi, Impact of heated wavy wall and hybrid nanofluid on natural convection in a triangular enclosure with embedded cold cylinder under inclined magnetic field, Arab. J. Sci. Eng. 50 (6) (2025) 4007–4020, https://doi.org/10.1007/s13369-024-09450-3.
[21] X. Zhao, Y. Leng, F. Nazir, J. Ahmed, A. Mohamed, I. Khan, M.A. Elkotb, Improved heat conduction in hybrid nanofluid across a slippery rotating cylinder with solar radiation and Lorentz forces, Ain Shams Eng. J. 16 (2) (2025) 103252, https://doi.org/10.1016/j.asej.2024.103252.
[22] F. Mebarek-Oudina, G. Dharmaiah, J.R. Prasad, H. Vaidya, M.A. Kumari, Thermal and flow dynamics of magnetohydrodynamic burgers' fluid induced by a stretching cylinder with internal heat generation and absorption, Int. J. Thermofluids 25 (2025) 100986, https://doi.org/10.1016/j.ijft.2024.100986.
[23] M.S. Junaid, M. Awais, M.N. Aslam, A.M. Zidan, M. Elamin, Thermal characteristics of jeffery hybrid nanofluid flow on a stretched cylinder: a comprehensive investigation into entropy generation and radiative heat transfer for engine oil optimization, Eur. Phys. J. Plus 139 (5) (2024) 460, https://doi.org/10.1140/epjp/s13360-024-05228-6.
[24] M. Faraz, J.M. Park, Thermal and MHD behavior of CNT Maxwell nanofluid over a stretchable cylinder, J. Radiat. Res. Appl. Sci. 18 (2) (2025) 101326, https://doi.org/10.1140/epjs/s11734-024-01425-7.
[25] A. Fayyaz, Z. Abbas, M.Y. Rafiq, Entropy generation for exact irreversibility analysis in the thermally radiative peristaltic flow of Williamson fluid through the annular region of eccentric cylinders, Eur. Phys. J. Spec. Top. 234 (1) (2025) 101–117, https://doi.org/10.1140/epjs/s11734-024-01425-7.
[26] P.V. Kumar, K. Jyothsna, S.M. Ibrahim, Insights into MHD flow of casson fluid over an exponentially permeable stretching surface using homotopy analysis method, Math. Comput. Sci. Real-World Appl. (2025) 251–282, https://doi.org/10.1002/9781394275359.ch16.
[27] U. Ali, M. Irfan, Study of gyrotactic motile microorganisms in powell-eyring nanofluid with non-fourier and non-fick's theories, J. Therm. Anal. Calorim. (2024) 1–17, https://doi.org/10.1007/s10973-024-13402-2.
[28] M. Sarfraz, M. Khan, Rheology of gyrotactic microorganisms in Jeffrey fluid flow: a stability analysis, Mod. Phys. Lett. B 38 (05) (2024) 2450003, https://doi.org/10.1142/S0217984924500039.
[29] D. Hussain, H. Huang, S. Shaheen, M.B. Arain, Study of gyrotactic microorganism with activation energy and thermal radiation on horizontal porous plate under variable wall temperature: sensitivity analysis, Int. Commun. Heat Mass Transf. 163 (2025) 108637, https://doi.org/10.1016/j.icheatmasstransfer.2025.108637.
[30] S. Bilal, K. Pan, A. Ullah, A. Anwar, A. Akgül, Aggregation of nanoparticles in flow of Carreau fluid containing gyrotactic microorganisms on extendable cylinder with viscous dissipation aspects by performing numerical simulations, Numer. Heat Transf. B: Fundam. 86 (3) (2025) 476–500, https://doi.org/10.1080/10407790.2023.2287590.
[31] S. Sun, S. Li, S. Shaheen, M.B. Arain, Usman, K.A. Khan, A numerical investigation of bio-convective electrically conducting water-based nanofluid flow on the porous plate with variable wall temperature, Numer. Heat Transf. A: Appl. 85 (22) (2024) 3791–3805, https://doi.org/10.1080/10407782.2023.2242579.
[32] M.I. Khan, A. Zeeshan, M.B. Arain, A.S. Alqahtani, M.Y. Malik, Temporal stability and non-unique solution of reacting Eyring Powell flows over shrinking wedges using neural networks, Eng. Appl. Artif. Intell. 141 (2025) 109828, https://doi.org/10.1016/j.engappai.2024.109828.
[33] D. Hussain, H. Huang, S. Shaheen, M.B. Arain, Study of gyrotactic microorganism with activation energy and thermal radiation on horizontal porous plate under variable wall temperature: sensitivity analysis, Int. Commun. Heat Mass Transf. 163 (2025) 108637, https://doi.org/10.1016/j.icheatmasstransfer.2025.108637.
[34] R. Baithalu, T.M. Agbaje, S.R. Mishra, S. Panda, Diversified characteristic of carbon nanotube nanoparticles on the entropy minimization for the flow of hybrid nanofluid through a convectively heated surface, ZAMM-J. Appl. Math. Mech./Z. Angew. Math. Mech. 104 (9) (2024) e202400259, https://doi.org/10.1002/zamm.202400259.
[35] K. Loganathan, P. Choudhary, S. Eswaramoorthi, K. Senthilvadivu, N. Thamaraikannan, R. Jain, Implications of entropy generation in bioconvective flow on Maxwell nanofluid past a Riga plate with Cattaneo–Christov model, Partial Differ. Equ. Appl. Math. 13 (2025) 101077, https://doi.org/10.1016/j.padiff.2025.101077.
[36] M.V. Reddy, K. Vajravelu, M. Ajithkumar, G. Sucharitha, P. Lakshminarayana, Numerical treatment of entropy generation in convective MHD Williamson nanofluid flow with Cattaneo–Christov heat flux and suction/injection, Int. J. Model. Simul. (2024) 1–18, https://doi.org/10.1080/02286203.2024.2405714.
[37] P.S. Reddy, P. Sreedevi, V.N. Reddy, Entropy generation and heat transfer analysis of magnetic nanofluid flow inside a square cavity filled with carbon nanotubes, Chem. Thermodyn. Therm. Anal. 6 (2022) 100045, https://doi.org/10.1016/j.ctta.2022.100045.
[38] S.U. Zaman, M.N. Aslam, A. Hussain, N.A. Alshehri, A.M. Zidan, Analysis of heat transfer in a non-Newtonian nanofluid model with temperature-dependent viscosity flowing through a thin cylinder, Case Stud. Therm. Eng. 54 (2024) 104086, https://doi.org/10.1016/j.csite.2024.104086.
[39] A. Jakhar, V.K. Sukariya, S. Kumar, A. Kumar, Anurag, Study of MHD Williamson fluid flow over a stretched cylinder with Hall, thermal dynamics, and chemical reactions effects, J. Therm. Anal. Calorim. (2024) 1–18, https://doi.org/10.1007/s40430-025-05504-1.
[40] O.D. Makinde, V. Nagendramma, C.S. Raju, A. Leelarathnam, Effects of Cattaneo-Christov heat flux on Casson nanofluid flow past a stretching cylinder, Defect Diffus. Forum 378 (2017) 28–38, https://doi.org/10.4028/www.scientific.net/DDF.378.28. Trans Tech Publications Ltd.
[41] R. Ullah, M. Israr Ur Rehman, A. Hamid, S. Arooj, W.A. Khan, Heat and mass transport aspect on magnetised Jeffery fluid flow over a stretching cylinder with the Cattaneo–Christov heat flux model, Mol. Phys. 122 (11) (2024) e2288701, https://doi.org/10.1080/00268976.2023.2288701.
[42] M.B. Ashraf, A. Tanveer, S. Ulhaq, Effects of Cattaneo-Christov heat flux on MHD Jeffery nano fluid flow past a stretching cylinder, J. Magn. Magn. Mater. 565 (2023) 170154, https://doi.org/10.1016/j.jmmm.2022.170154.
[43] M.N. Khan, N. Ahsan, M. Hussien, T. Saidani, F.M. Aldosari, H.F. Alrihieli, Heat and flow analysis of a bioconvective second-grade nanofluid with multiple slip effect over a stretching porous cylinder, Case Stud. Therm. Eng. 70 (2025) 106073, https://doi.org/10.1016/j.csite.2025.106073.